VALUE: COST Action ES1102

Validation for physical processes I+II

Pedro M.M. Soares (Instituto Dom Luiz, University of Lisbon
Douglas Maraun (Wegener Center, University of Graz)

pmsoares@fc.ul.pt
douglas.maraun@uni-graz.at

4th COST VALUE training school | 26 - 30 October 2015 | Trieste, Italy

Motivation

Dynamical Downscalling

Most of Regional Climate Modellers look only to surface errors

but models are based on physics and represent atmospheric circulations: both should be looked at…

Statistical Downscalling

based on empirical relationships and the behaviour depency on circulation regimes (e.g.) should be inspected

Isolating Processes

a number of evaluation techniques to achieve both process and component isolation

1. **Regime-oriented**

- circulation regimes
- cloud regimes
- thermodynamic states

results are averaged within categories that describe physically distinct regimes of the system

2. **Model components or parameterizations** - isolation of model components or parameterizations in simulations, including SCMs of the atmosphere:

- Numerous evaluation studies have been done on climate model processes

- Feedback analysis: partial radiative perturbation method (PRP, Wetherald and Manabe 1988), or the online feedback suppression method (Hall and Manabe 1999) and the coupled atmosphere–surface climate feedback–response analysis method (CFRAM) (Lu and Cai 2009)

- Sensitivity experiments

1. Circulation regimes

Ability of an ensemble of regional climate models to reproduce weather regimes over Europe-Atlantic during the period 1961–2000

ENSEMBLES RCMs

25km; 50km

ERA-40

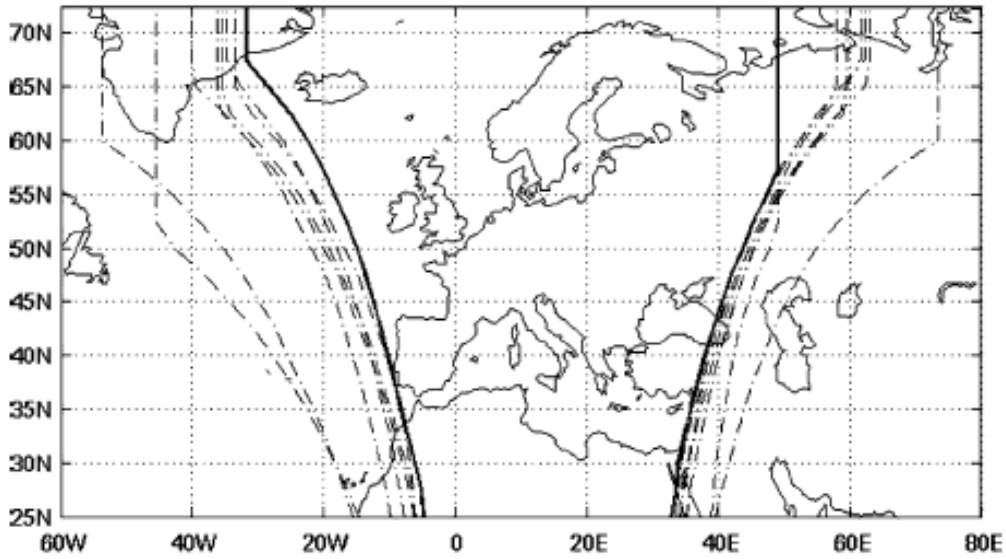

Table 1 Summary of the main features of the regional climate models participating in the FP6 ENSEMBLES project

Institution	RCM	Grid points	Vertical levels	References
CHMI	ALADIN	83 × 95	27	Farda et al. (2007)
CNRM	ALADIN	93 × 101	31	Radu et al. (2008)
DMI	HIRHAM	90 × 95	31	Christensen et al. (1996)
ETHZ	CLM	91 × 97	32	Böhm et al. (2006)
GKSS	CLM (spectral nudging)	95 × 85	32	Böhm et al. (2006)
ICTP	RegCM	98 × 86	34	Giorgi and Mearns 1999.
KNMI	RACMO	95 × 85	40	Lenderik et al. (2003)
METNO	HIRHAM	85 × 95	31	Haugen and Haakensatd (2006)
METOHC	HadRM	115 × 118	19	Collins et al. (2006)
MPI	REMO	85 × 95	27	Jacob (2001)
SMHI	RCA	85 × 95	24	Kjelltröm et al. (2005)
UCLM	PROMES	90 × 104	28	Sanchez et al. (2004)
OURANOS	CRCM	91 × 91	28	Plummer et al. (2006)

Sanchez-Gomez et al. 2009

Weather Regime Methodology

Principal Component Analysis is performed on the Z500 anomalies

the first 15 principal components which explain about 90% of the total variance are kept

k-means cluster algorithm; the number of groups is a priori unknown and a Monte–Carlo test is needed to determine the optimal number k of clusters

k = 4 - patterns corresponding to the well-known North Atlantic weather regimes

Weather regimes are represented as the composites of Z500 anomalies, obtained by averaging over all the days for the same weather regime

Sanchez-Gomez et al. 2009

- The Blocking regime (BL) displays a strong blocking cell over Scandinavia
- The Zonal regime (ZO or NAO+)
- The Atlantic Ridge (AR) regime presents a positive anomaly over the North Atlantic basin
- The Greenland Anticyclone (GA or NAO-) exhibits a strong positive anomaly centred over west of Greenland

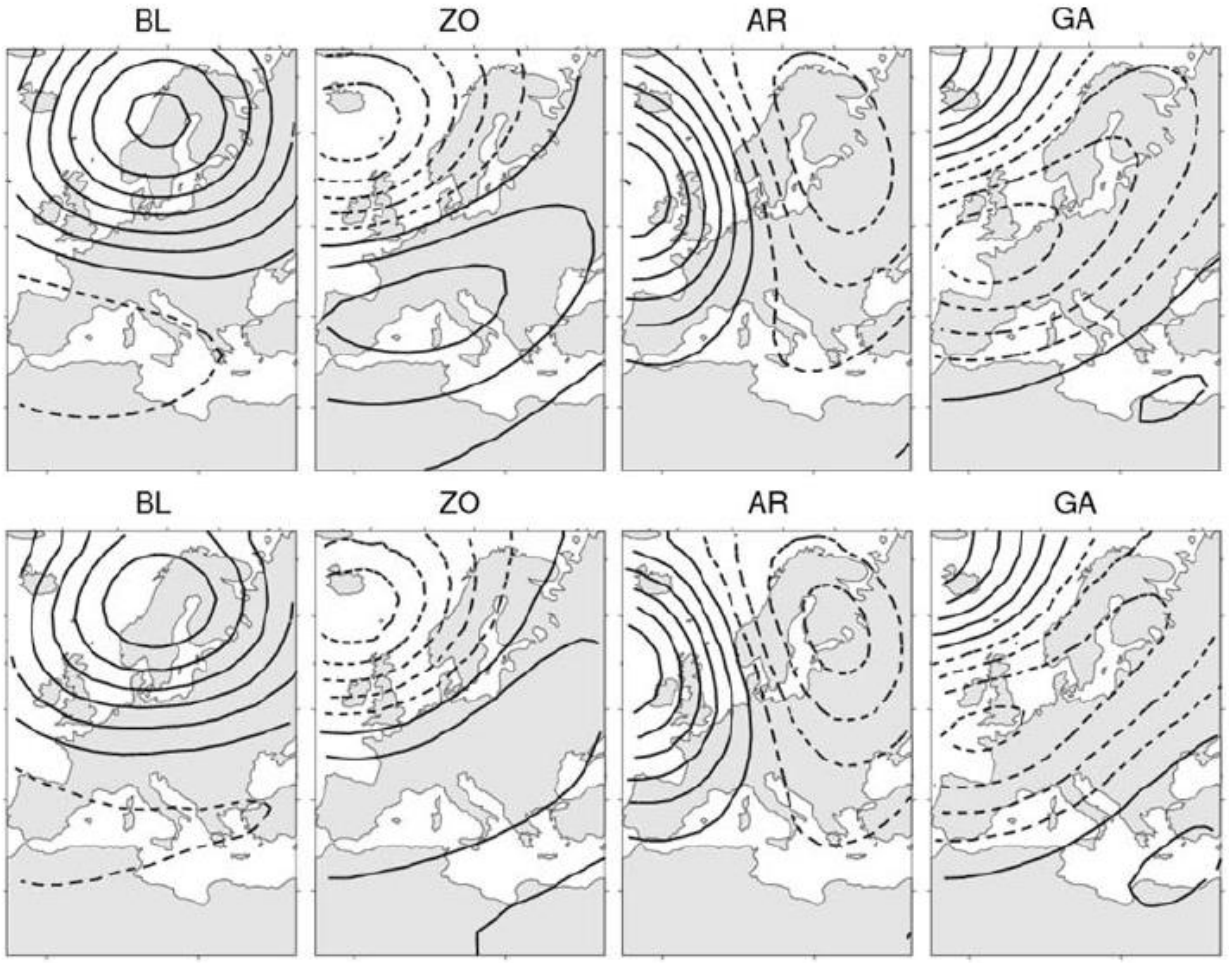

Composites of the North Atlantic weather regimes in winter for ERA40 (top) and CNRM model (bottom). The isolines are the Z500 anomaly composite (solid lines are positive and dot dashed are negative values). Contour interval is 30 gpm

Sanchez-Gomez et al. 2009

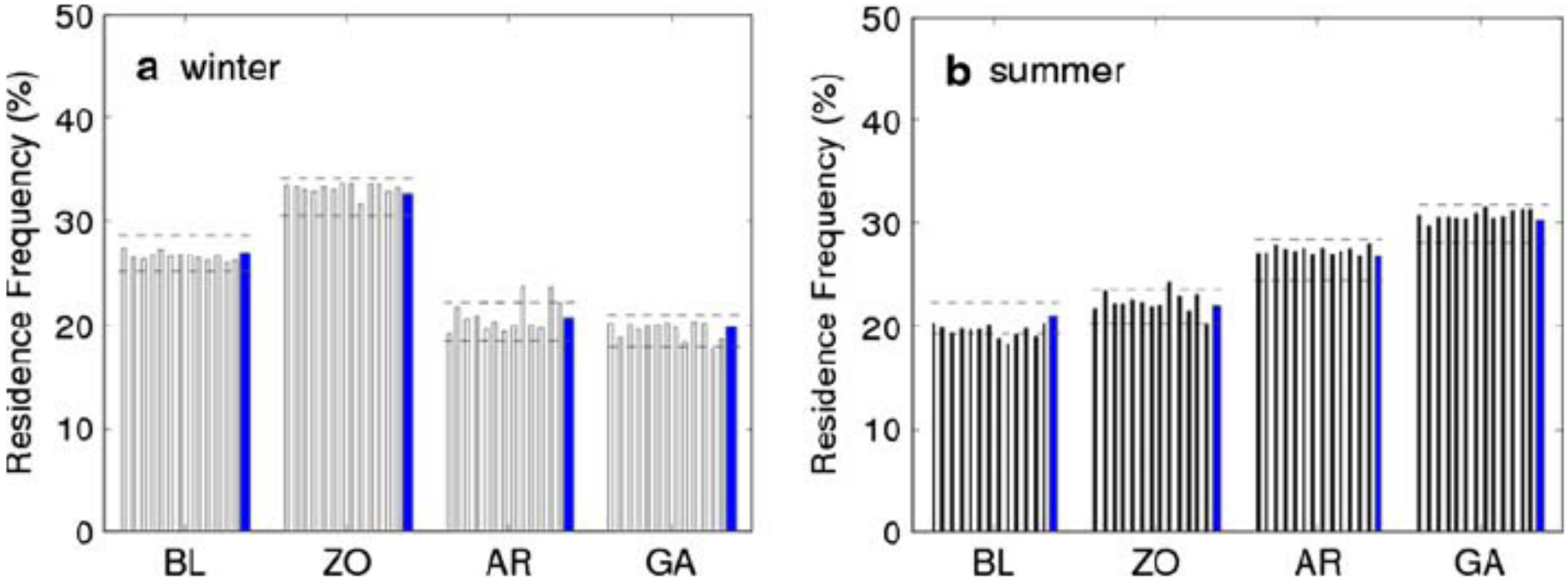

Fig. 3 Mean frequency of occurrence of each weather regime computed as the average over all winters (a) and summers (b) within the time period 1961–2000. Slim bars correspond to RCMs weather regimes and block bar corresponds to ERA40 reanalysis.

Sanchez-Gomez et al. 2009

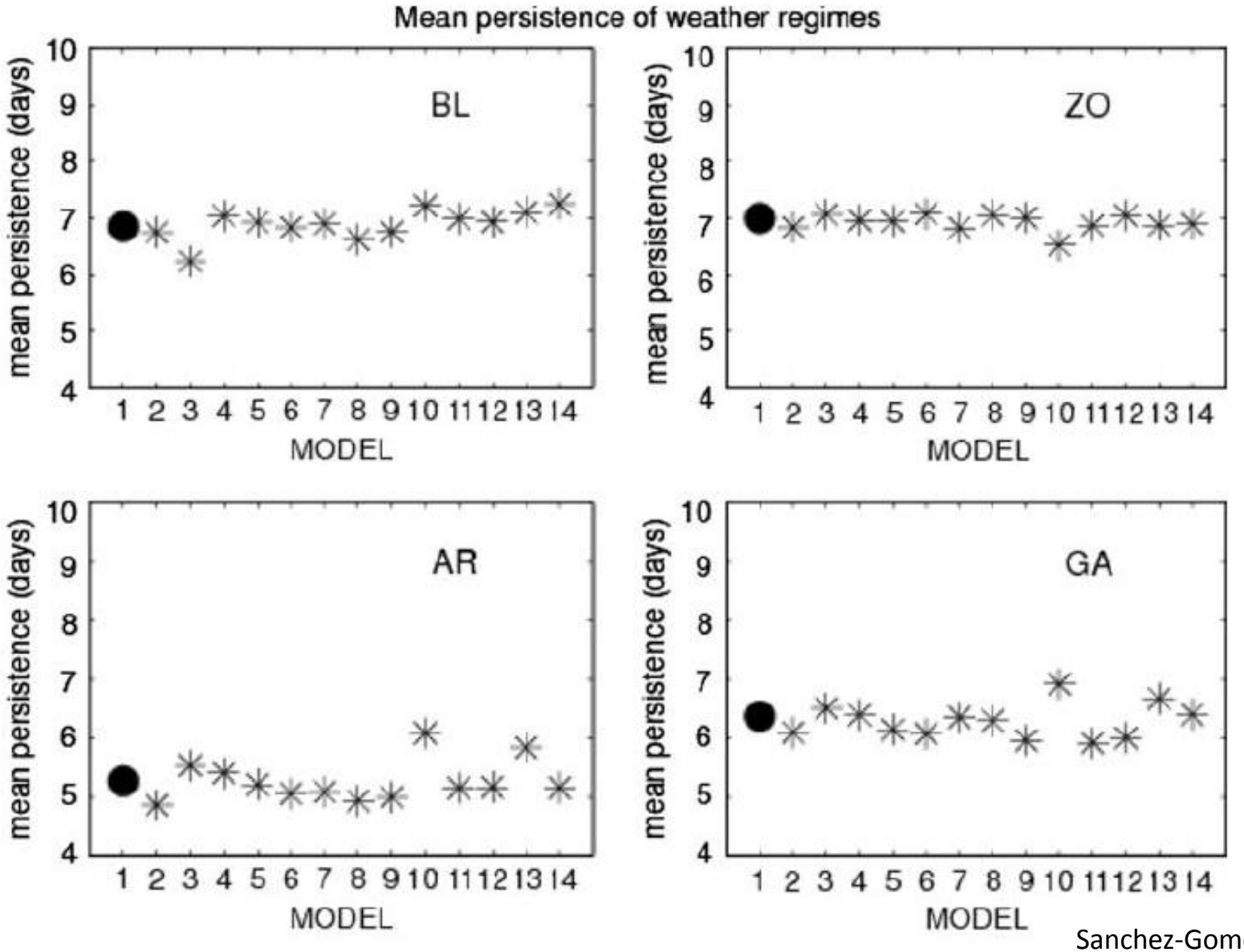

Sanchez-Gomez et al. 2009

Fig. 4 Mean persistence values (in days) of the four weather regimes in the winter period for ERA40 (big dot) and the RCMs (stars).

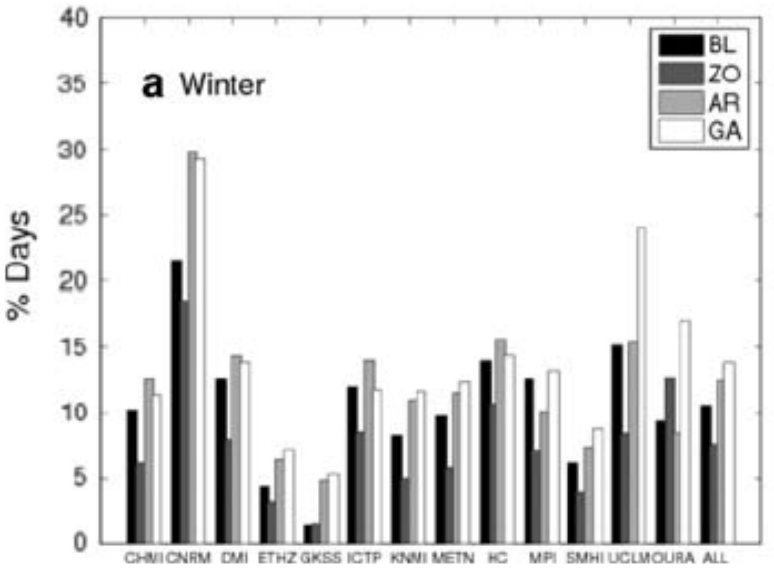

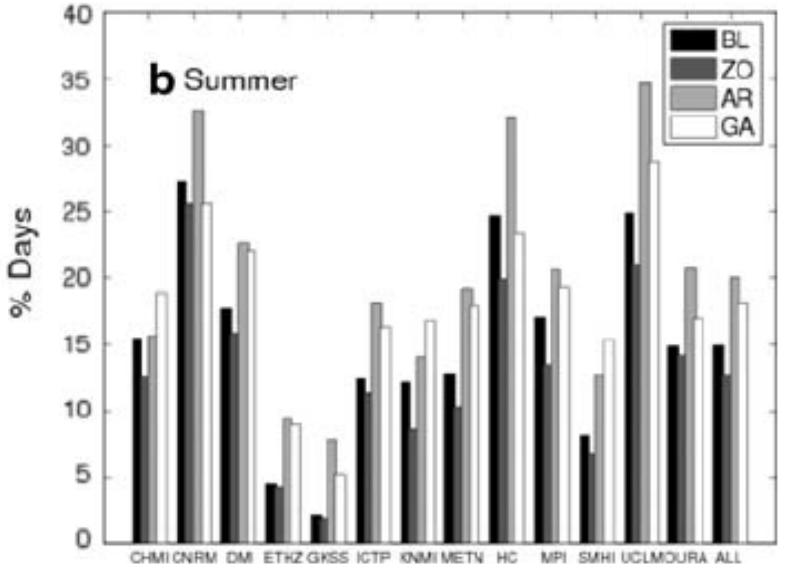

total number of wrong 10.2% winter 17% summer

Fig. 7 Percentage of ‘‘wrong’’days in which the RCMs are not in the same weather regime as ERA40 (the driving field). ALL represents the ensemble mean, excluding the GKSS model

Sanchez-Gomez et al. 2009

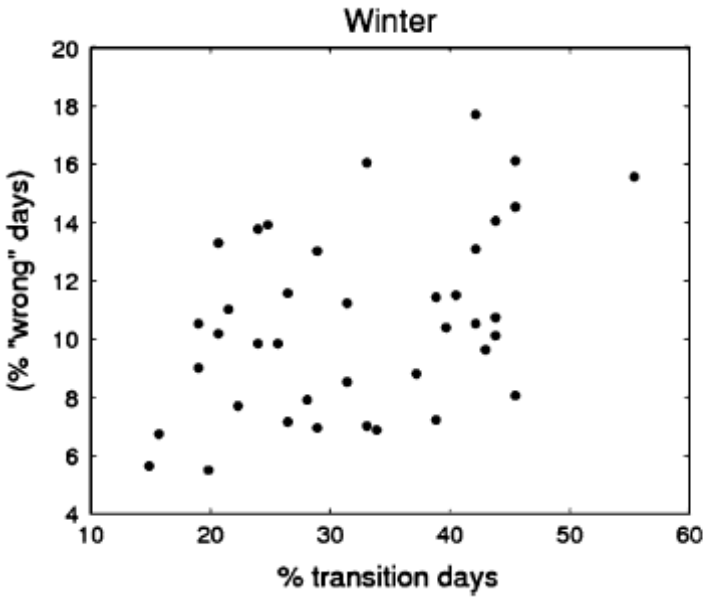

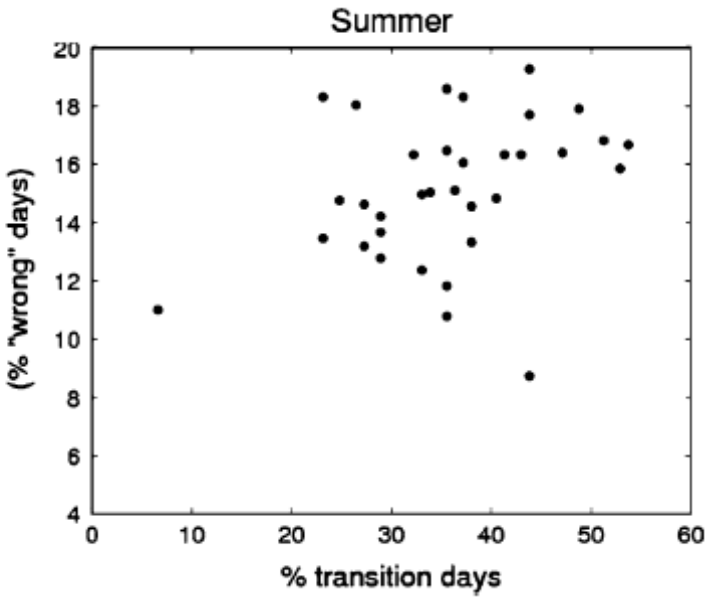

Fig. 8 Scatter plots showing the percentage of ‘‘wrong’’ days per year versus the number of days of weather regimes transitions (in percentage)

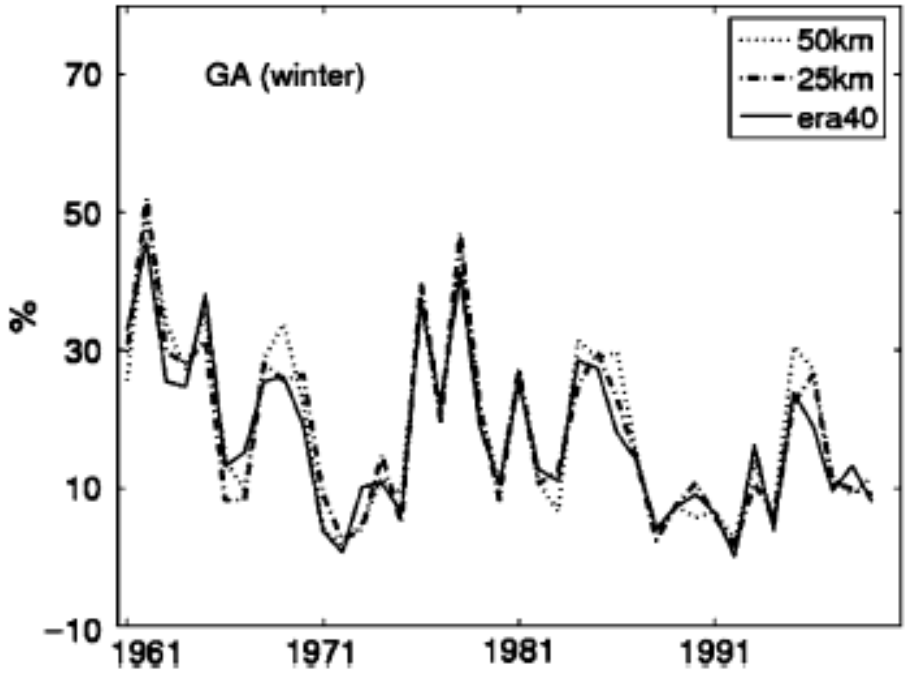

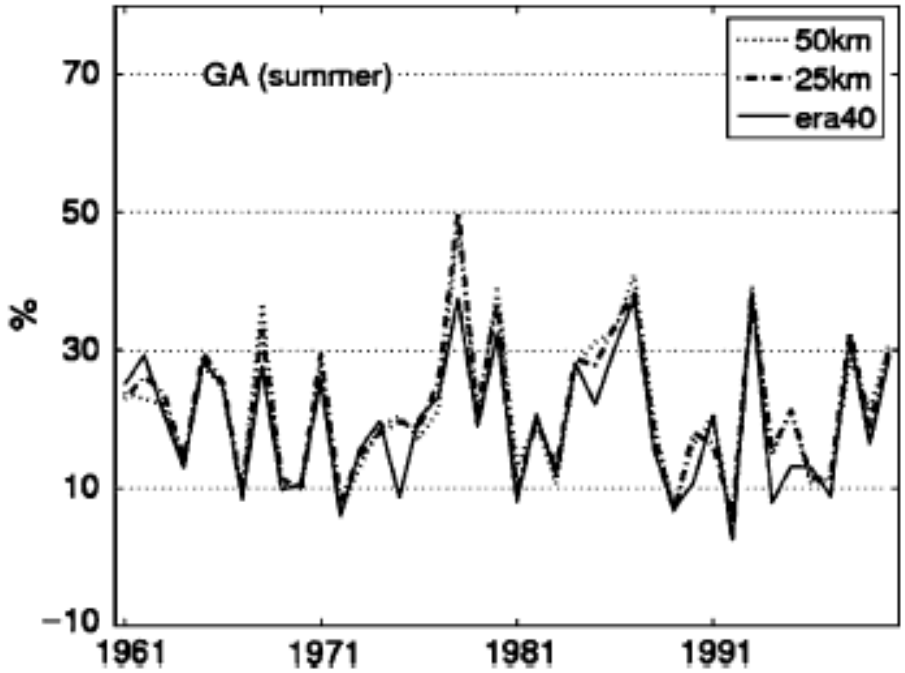

Fig. 9 Annual time series of the frequency of occurrence of the Greenland anticyclone (GA) weather regime for the CNRM model for winter and summer periods.

RCMs reproduce very well the composite pattern, the mean frequency of occurrence of weather regimes as well as the mean persistence values.

Largest domain size are penalized

Day-to-day correspondence between the weather regimes in ERA40 and in the RCMs, the discrepancies among the models are more evident

There are nested models which significantly degrade the large-scales of ERA40

In summer all models degrade significantly

Sanchez-Gomez et al. 2009

The weather regimes associated with the largest error are the GA for winter and AR for summer.

In both seasons the ZO regime exhibits the smallest errors

The percentage of ‘‘wrong’’ days is somewhat related to the number of transitions days between the weather regimes for a given season

Following these results, one should be cautious in a **statistical downscaling** scheme that proposes the large-scale solution generated by a RCM as a daily predictor field.

The model performance to reproduce the large-scale conditions of ERA40 improves significantly with the spectral nudging

Sanchez-Gomez et al. 2009

But let’s go back for GCMs…

The same GCM at different resolutions is consistent on generating the weather regimes???

Simulating regime structures in weather and climate prediction

daily fields of wintertime (December–March; **DJFM**)
geopotential height on the 500 hPa pressure surface

ECMWF Integrated Forecast System (IFS) Cycle 36r1

high resolution at T1279 resolution
low resolution at T159 resolution

16 km and 125 km

45-year period 1962–2006

vs

ERA
ECMWF 40-year reanalysis
(ERA-40; 1962–1988) and

ECMWF interim reanalysis
ERAInterim; 1989–2006)

Dawson et al. 2012

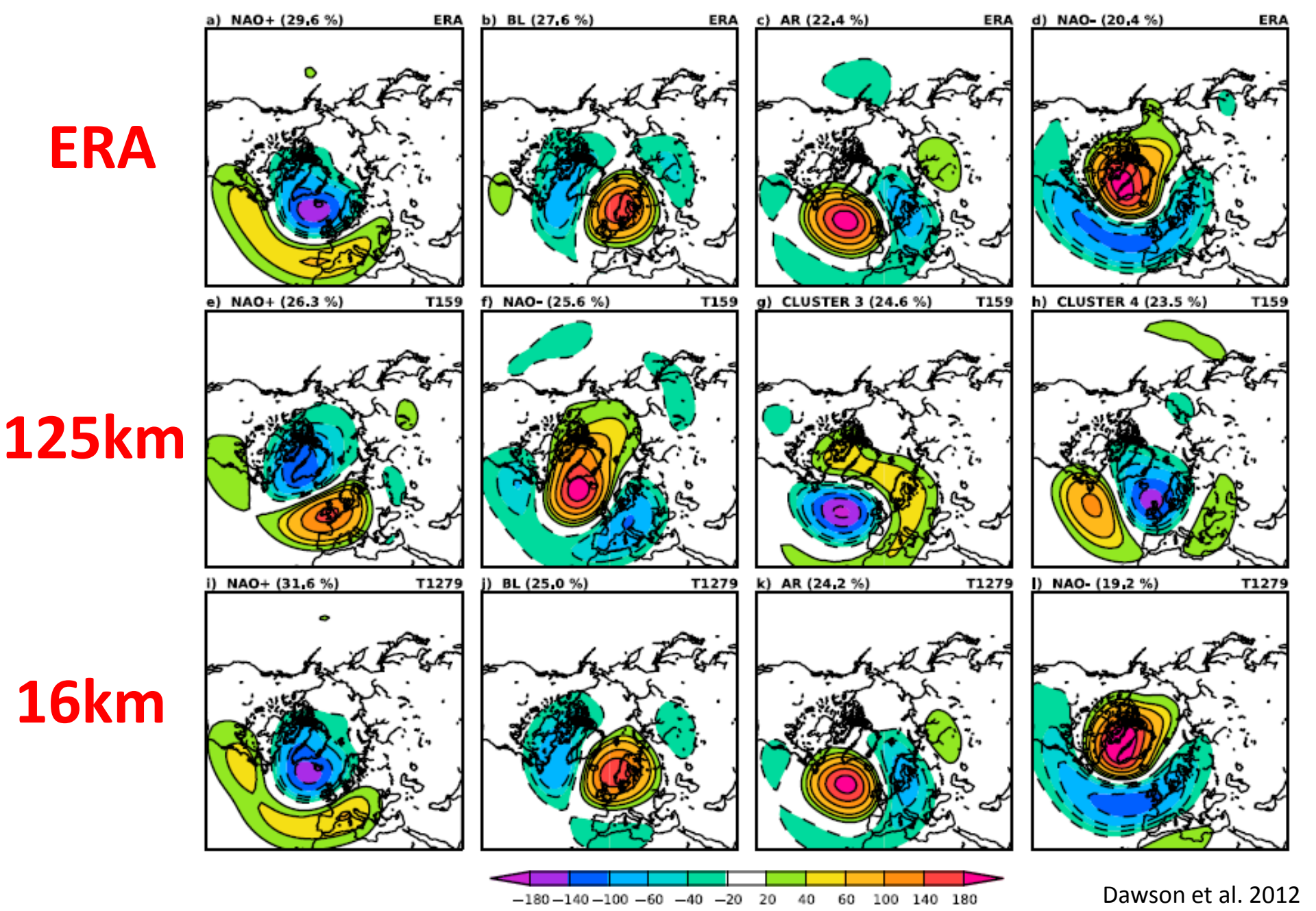

Figure 1. Cluster centroid maps of 500 hPa geopotential height.

Table 2. Transition Probabilities for ERA[a]

	NAO+	BL	AR	NAO−
NAO+	–	0.41	0.43	0.16
BL	0.38	–	0.31	0.31
AR	0.46	0.33	–	0.21
NAO−	0.29	0.34	0.37	–

[a]Probabilities of transitioning from a given regime (rows) into each of the other regimes (columns).

Table 3. Transition Probabilities for the T1279 Model Configuration[a]

	NAO+	BL	AR	NAO−
NAO+	–	0.43	0.43	0.15
BL	0.45	–	0.32	0.22
AR	0.40	0.34	–	0.25
NAO−	0.31	0.30	0.40	–

[a]As Table 2.

Dawson et al. 2012

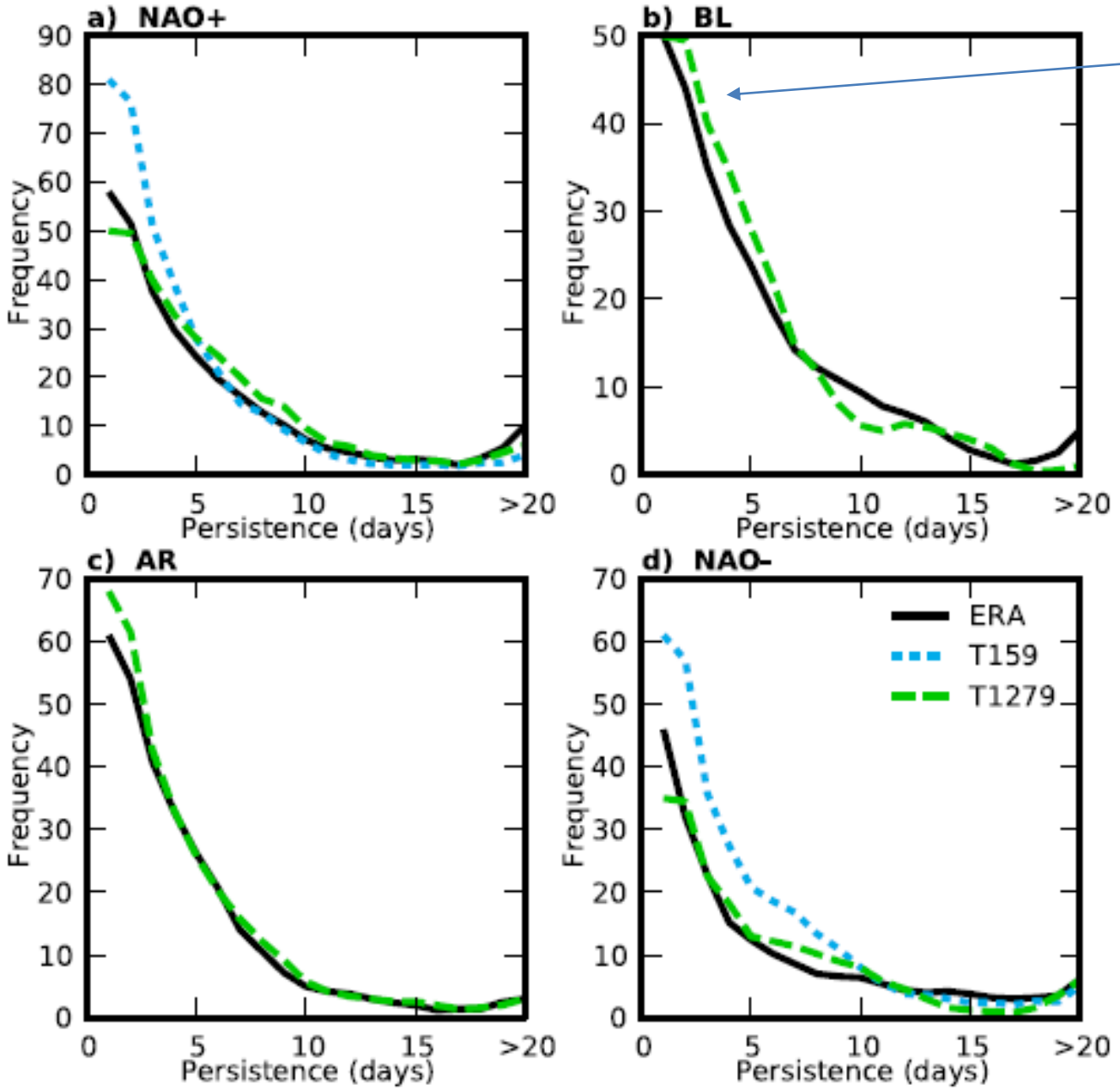

Dawson et al. 2012

- The high resolution model configuration has clusters similar to those in ERA, with a high level of significance.

- The temporal characteristics of the clusters are similar to ERA, with the exception of the blocking cluster, which appears to be visited for more short periods and fewer longer periods than in ERA.

- **The low resolution model configuration does not have a realistic representation of regimes in the European/Atlantic sector.**

- This configuration identifies the positive and negative phases of the NAO as clusters, but the significance of the clusters is low.

- **A low resolution atmospheric model, with horizontal resolution typical of CMIP5 models, is not capable of simulating the statistically significant regimes seen in reanalysis**

Dawson et al. 2012

How this impacts on surface properties like precipitation and temperature?

Responses of European precipitation distributions and regimes to different blocking locations

NCEP/NCAR reanalysis

locations of the Z500 maximum anomaly for each identified blocking pattern are called blocking centers

daily precipitation data for Europe from the E-OBS dataset during the period 1950-2012

Sousa et al. 2015, submitted

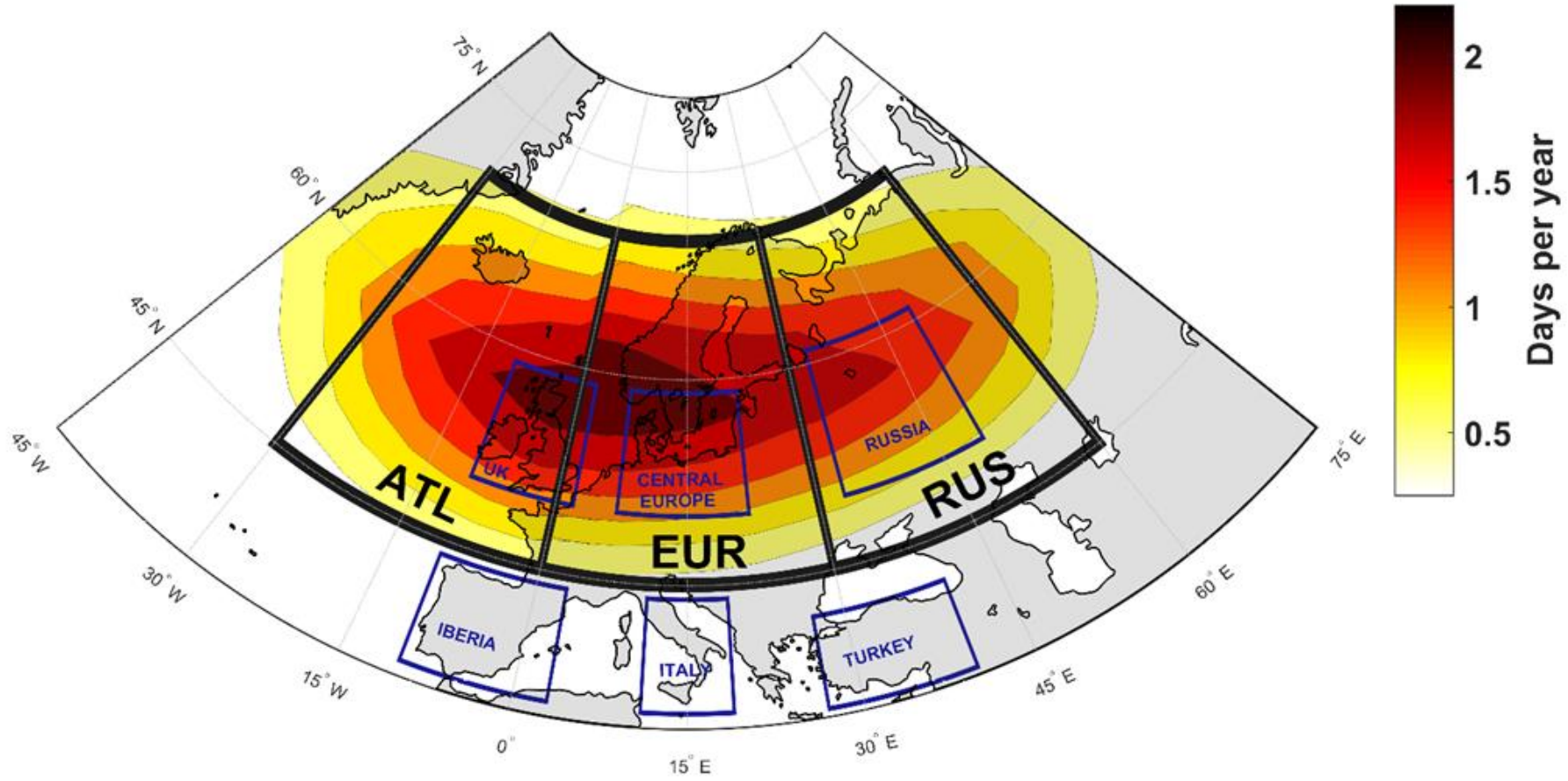

Fig.1- Thick black boxes identify the considered sectors for blocking center location: Atlantic (ATL) – from 30W to 0W; European (EUR) – from 0E to 30E; Russian (RUS) – from 30E to 60E. The shadings indicate the annual mean frequency of blocking center locations in each gridpoint. Blocks outside the 45N to 70N latitude strip were discarded in both sectors. Thin blue boxes identify areas which were considered in the regional assessment performed in Section 5.

Sousa et al. 2015, submitted

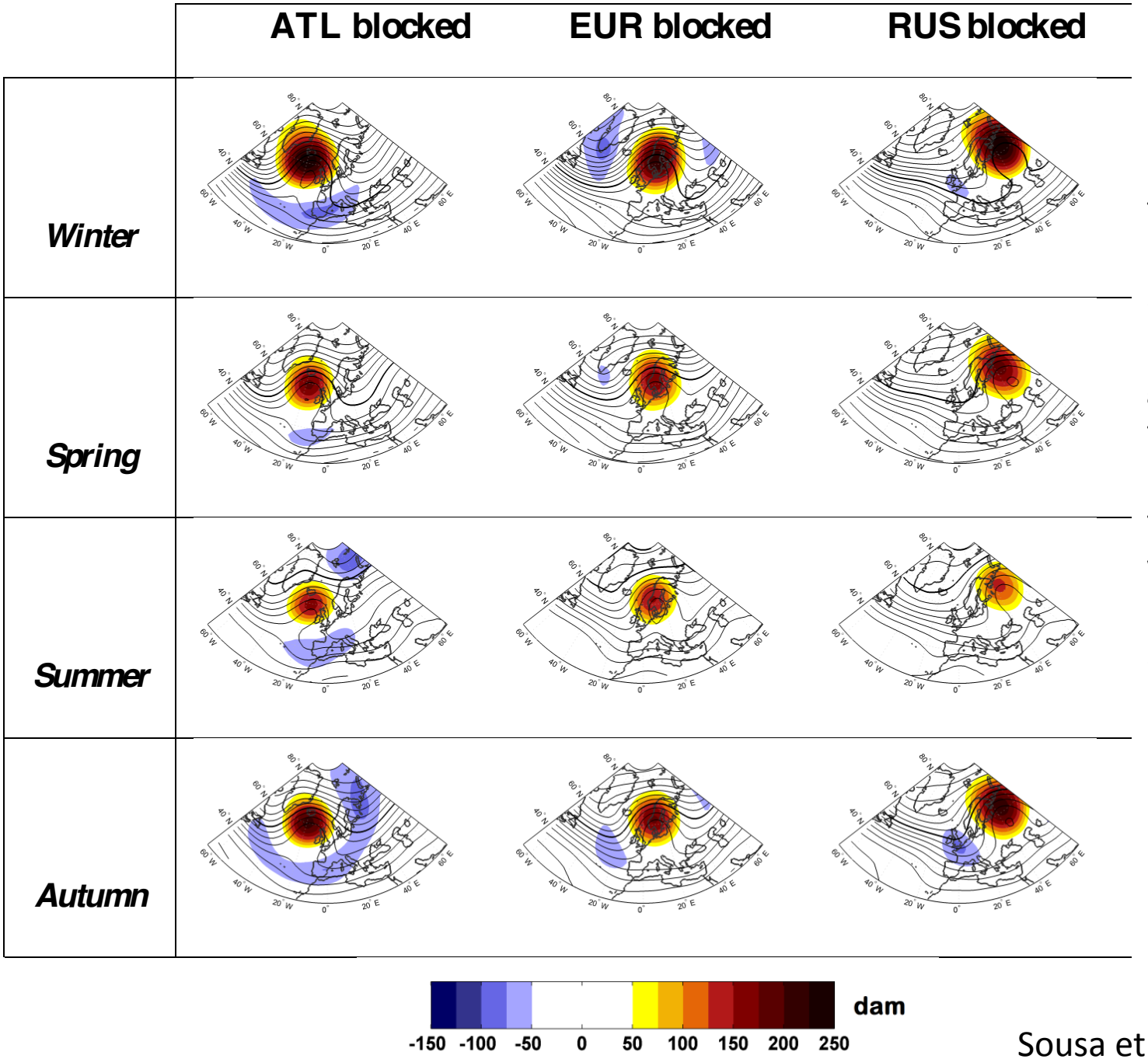

Fig.2- Composites of the daily anomalies (shaded areas) and absolute values (isolines) of 500 hPa geopotential height for blocking centers in each sector and for all seasons. All values are in decameters (dam) and the thick line represents the 550 dam isohypse.

Sousa et al. 2015, submitted

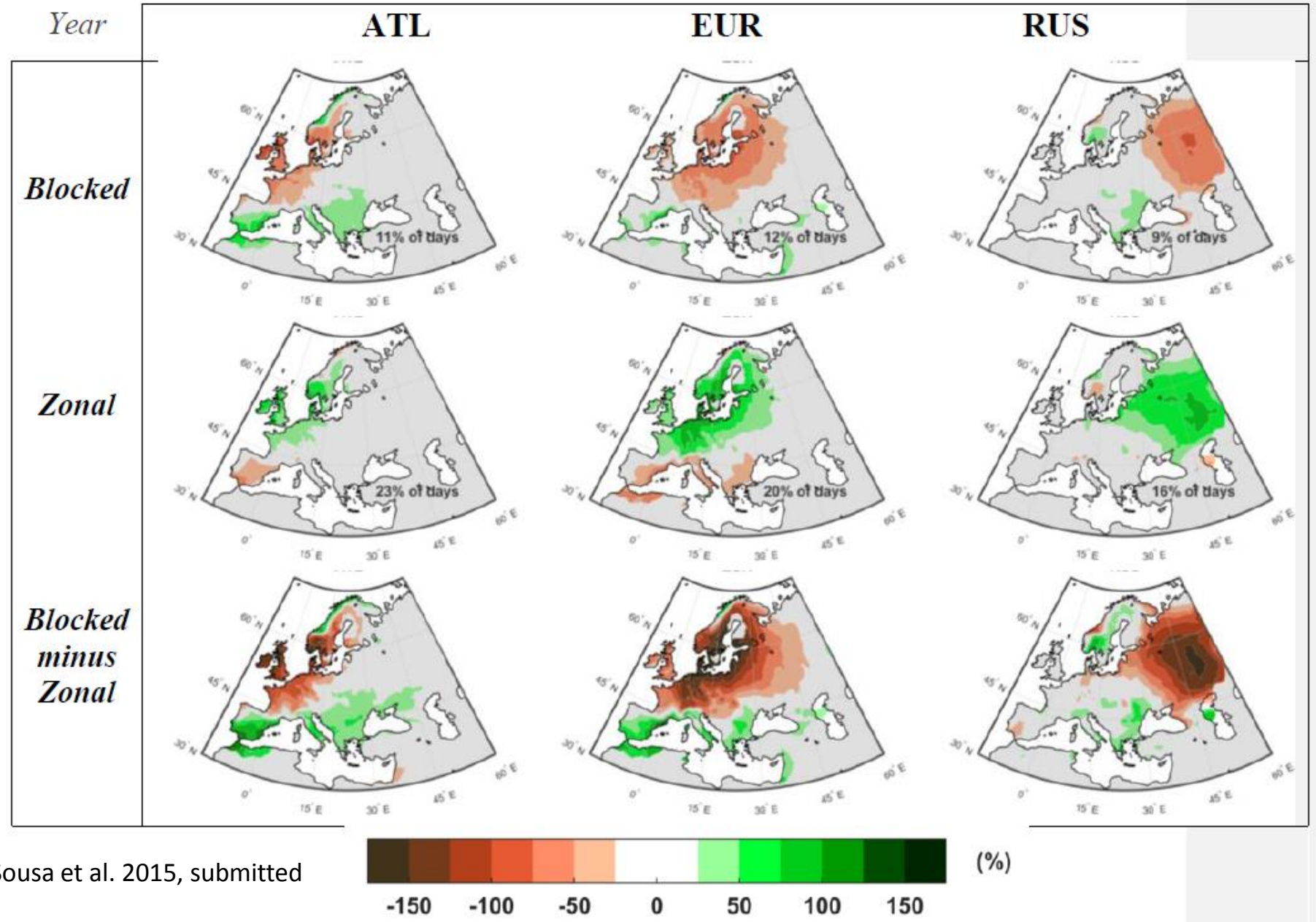

Sousa et al. 2015, submitted

Fig.3- Annual composites for daily precipitation anomalies (%) in Europe during blocking (upper row) and strong zonal flow (middle row) days in the ATL (left column), EUR (central column) and RUS (right column) sectors. The difference between the regional blocking and strong zonal

5. Shifts in precipitation distributions

Sousa et al. 2015, submitted

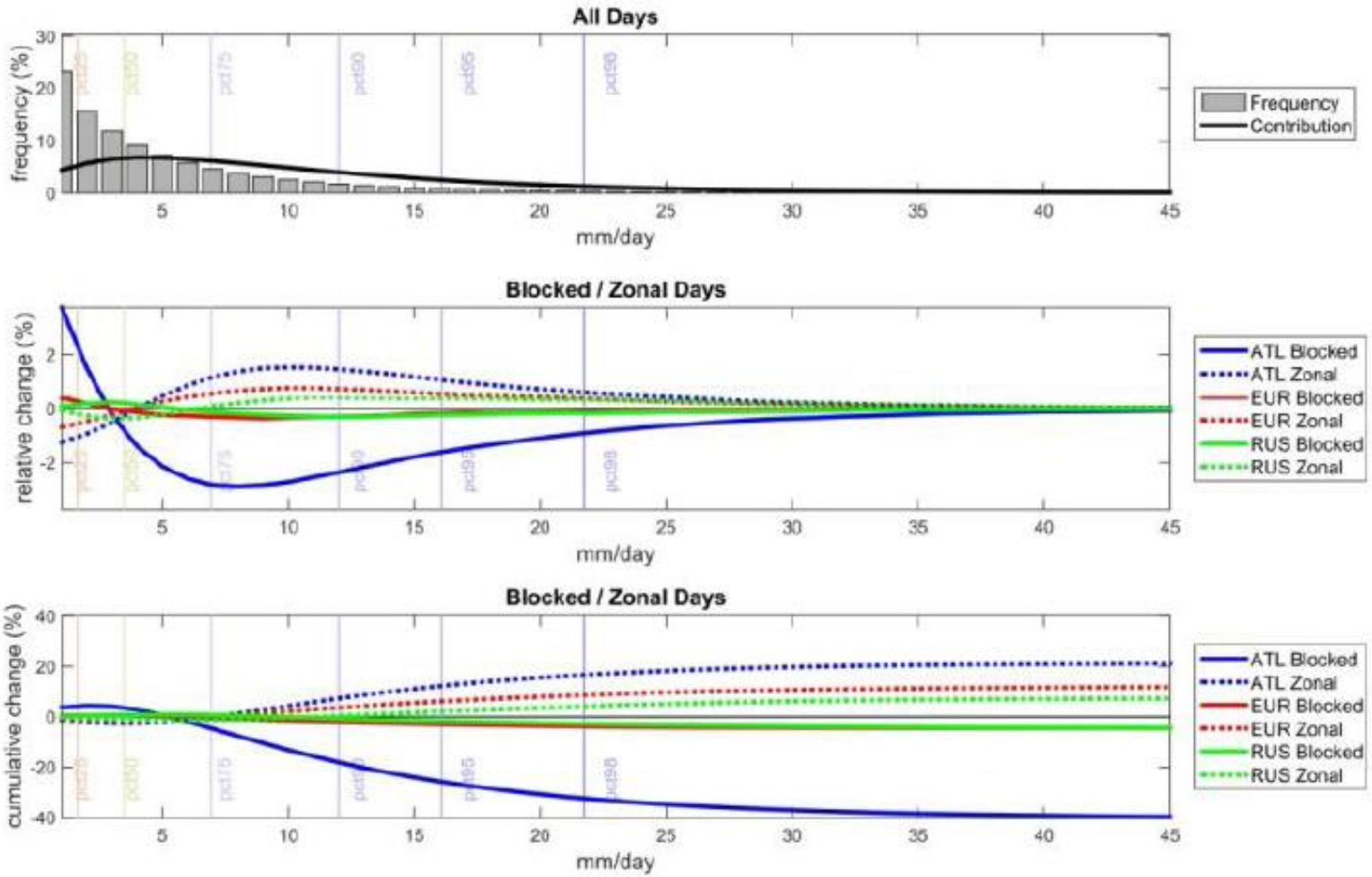

Fig.9- Changes in the precipitation distribution of the UK during the different considered synoptic patterns. Top: Relative frequency of days with precipitation totals, considering 1mm bins (grey bars) and the corresponding contribution of each bin to the total annual precipitation (solid black line). Middle: Relative change in the contribution of each bin to the total annual precipitation for blocked (solid lines) and zonal (dashed lines) patterns in the three considered

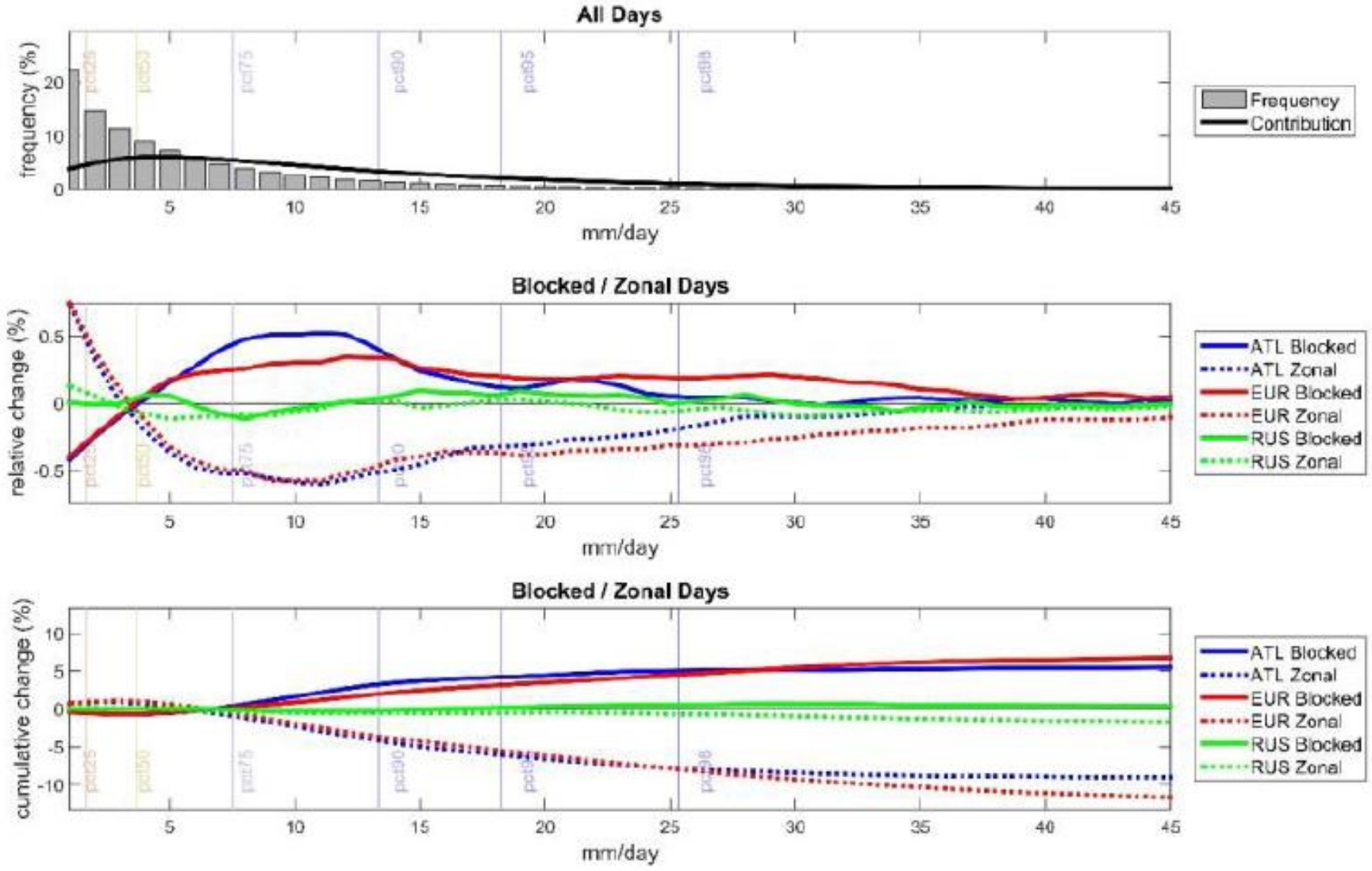

Fig.10- Same as Fig.9, but for the Iberian Peninsula.

Sousa et al. 2015, submitted

European temperatures in CMIP5: origins of present-day biases and future uncertainties

33 models participating to CMIP5

1979–2008 in historical simulations
(HIST)

2070–2099 in simulations under the 8.5 W/m2

Cattiaux et al. (2013)

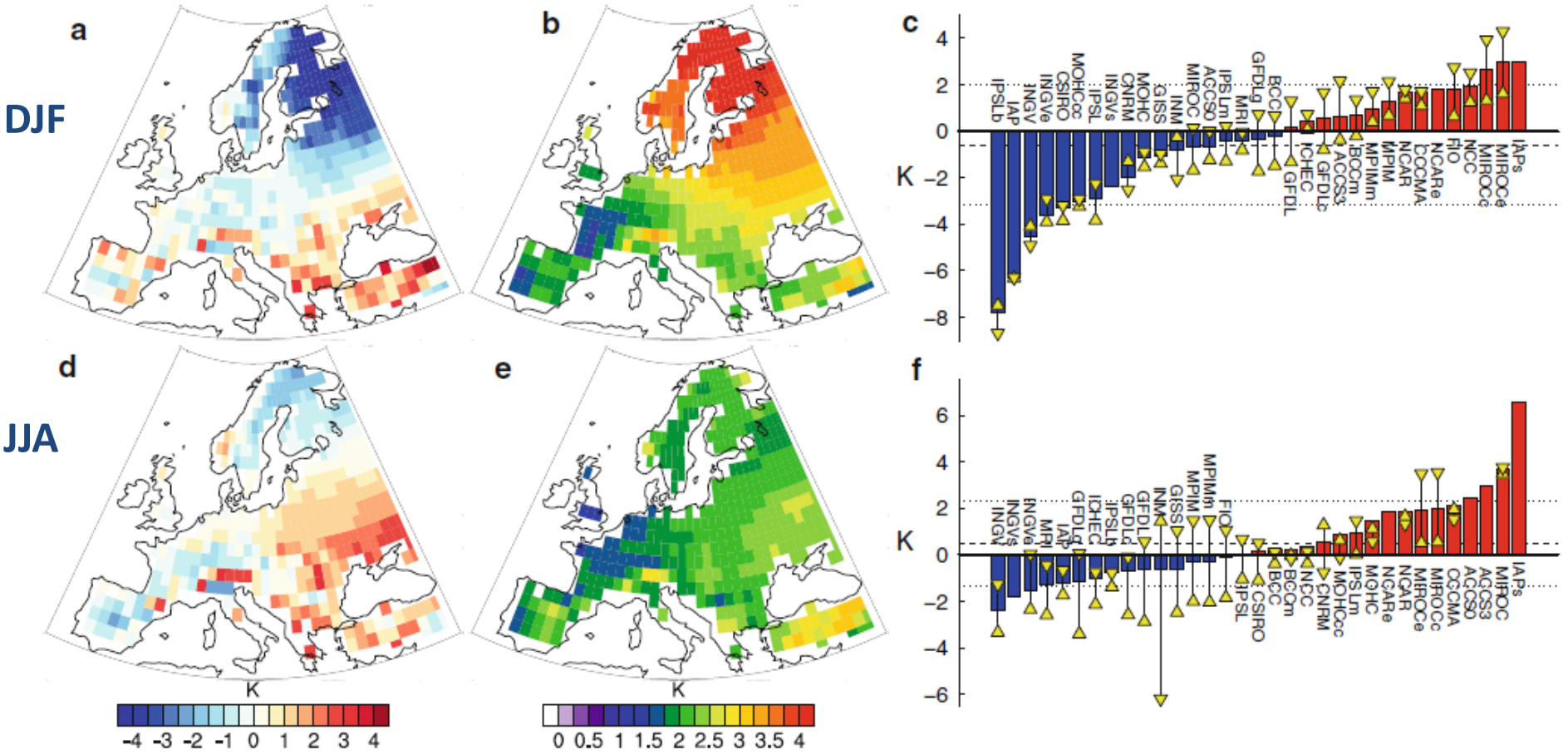

Cattiaux et al. (2013)

a Ensemble-mean temperature bias relative to EOBS.
b Inter-model standard deviation (r).
c Individual model biases averaged over continental Europe (i.e. grid points in a and b), and sorted by increasing order. Ensemble mean (dashed line) and ±1r departures (dotted lines) are added. Upward (downward) triangles indicate corresponding values for daily maximum (minimum) temperatures, when available

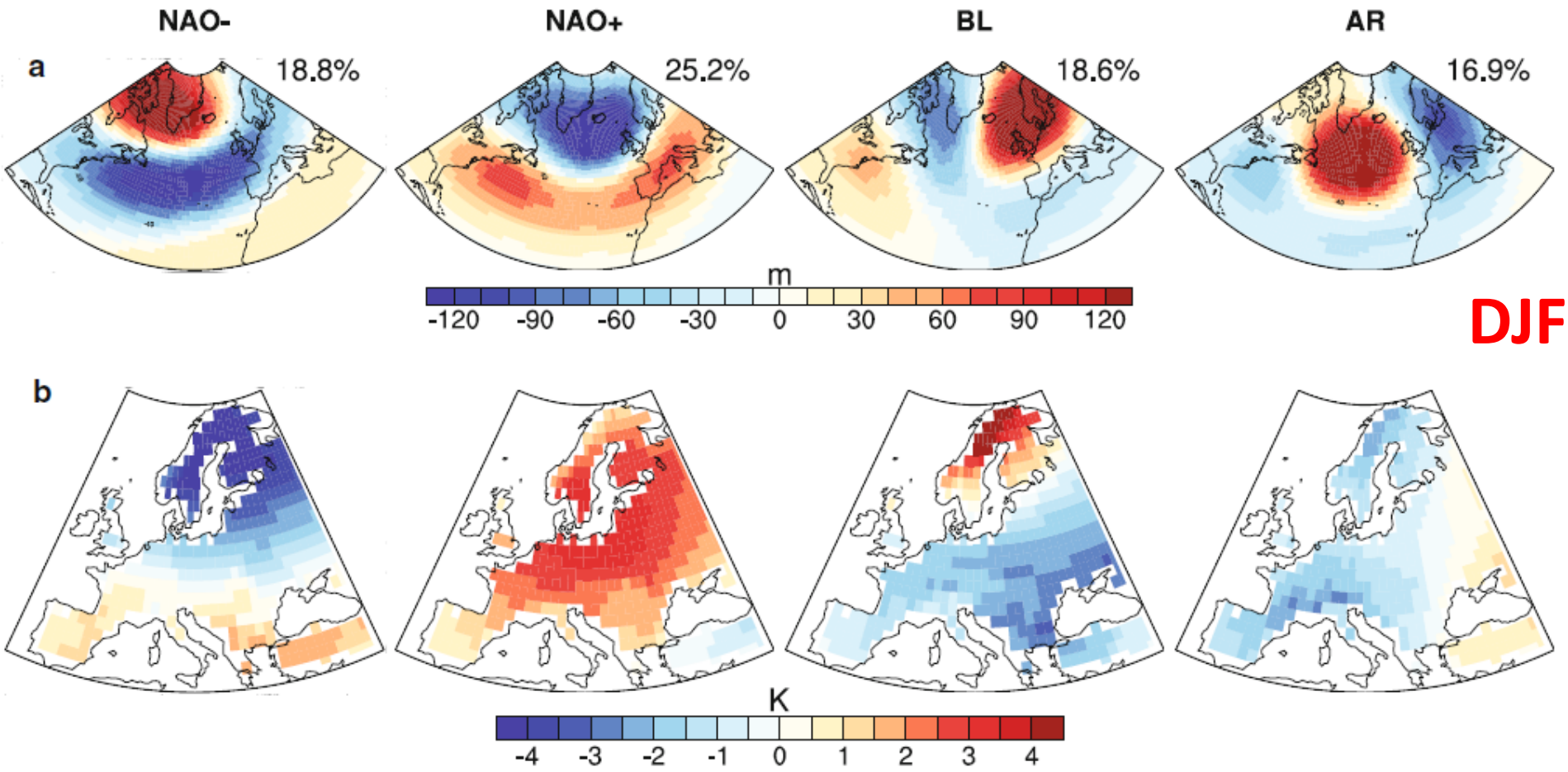

a Composites of Z500 anomalies (**NCEP2**) corresponding to winter weather regimes: NAO-, NAO+, Blocking (BL) and Atlantic Ridge (AR). Mean frequencies of occurrence are indicated, and do not sum as 1 because of days placed in the bin class.

b Composites of temperature anomalies (EOBS)

Cattiaux et al. (2013)

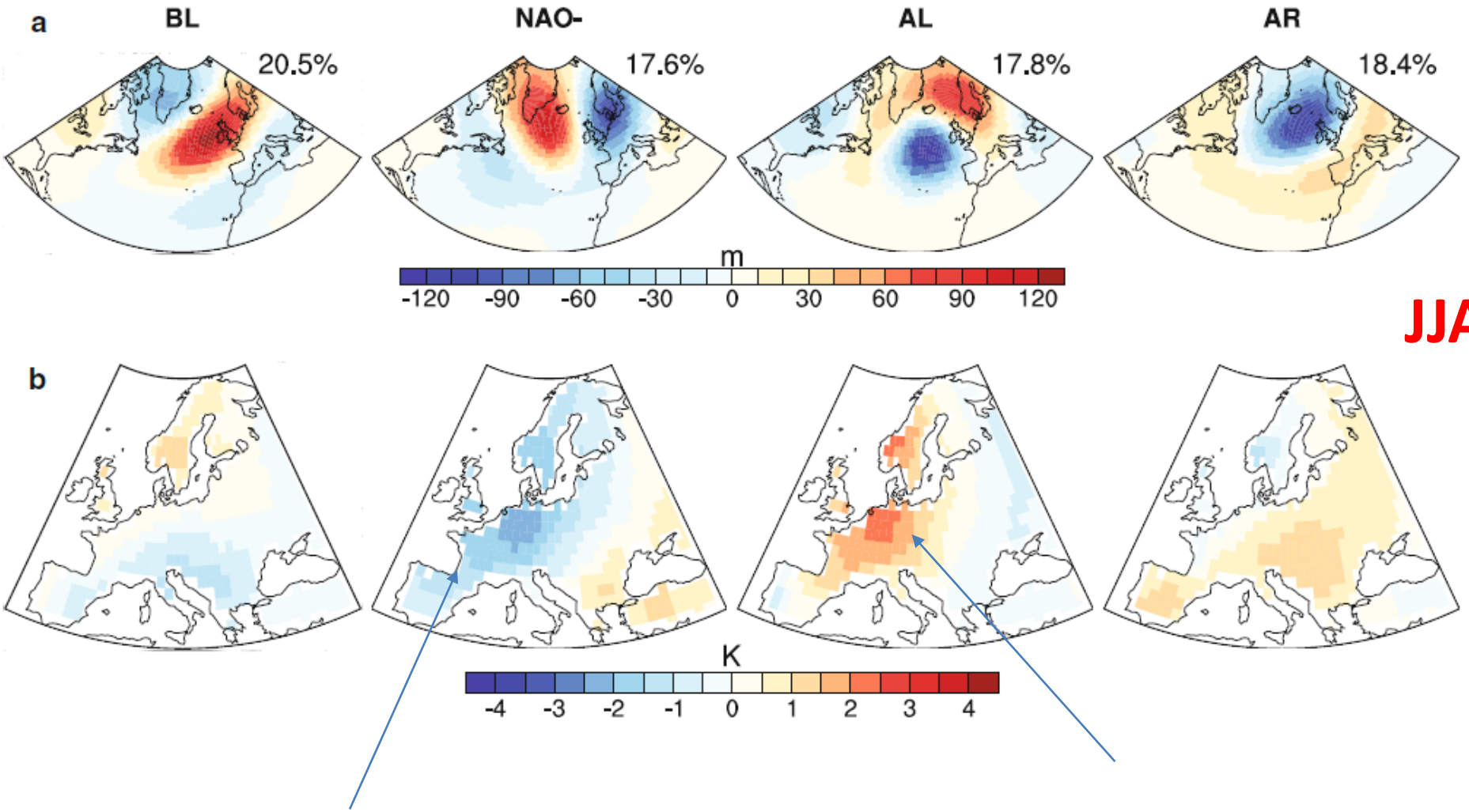

Fig. 6 Same as Fig. 5 for summer weather regimes:
Blocking (BL), NAO-, Atlantic Low (AL) and Atlantic Ridge (AR)

Cattiaux et al. (2013)

Mean temperature anomaly T' can be written as the mean of regimes' composites tk weighted by the regimes' frequencies fk

$$\overline{T'} = \sum_k f_k \cdot \phi(z_k) = \lfloor f \cdot \phi(z) \rfloor_k .$$

Thus, the difference between two mean temperature anomalies (i.e. biases between models and observations, or changes between HIST and RCP85) can be broken down according to:

$$\Delta\overline{T} \sim \underbrace{\lfloor \Delta f \cdot \phi(z) \rfloor_k}_{BC} + \underbrace{\lfloor f \cdot \phi(\Delta z) \rfloor_k}_{WCd} + \underbrace{\lfloor f \cdot \Delta\phi(z) \rfloor_k}_{WC\phi} + \varepsilon,$$

with BC the contribution of regimes' frequencies (Between-Class), WCd the contribution of regimes' circulations (Within-Class, dynamics), Wc(phi) the contribution of the transfer function (Within-Class, physics), and e a second-order residual.

BC and WCd - account for biases/changes in large-scale dynamical regimes

Cattiaux et al. (2013)

WC(phi) represents temperature biases/changes for equal circulations

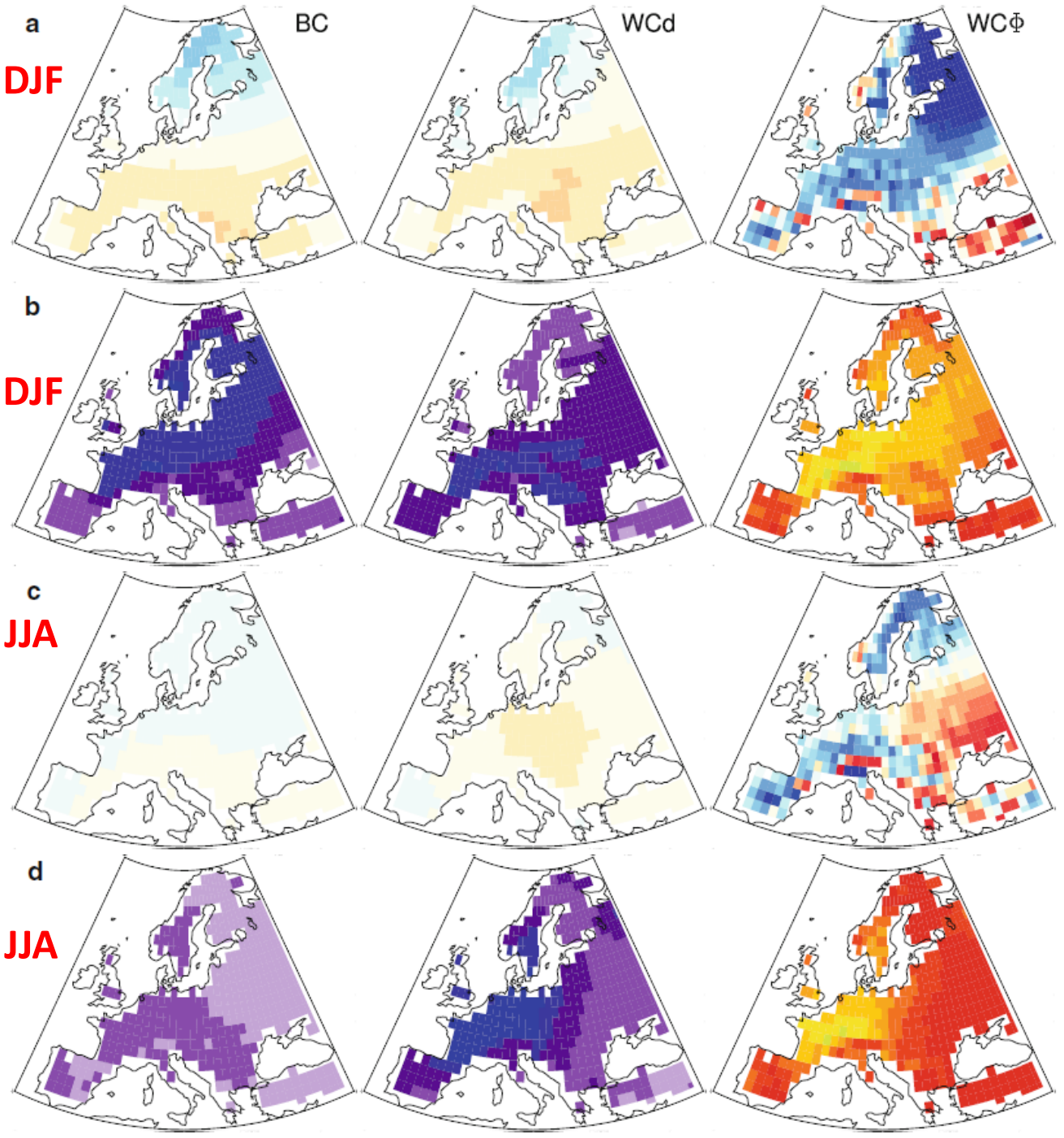

Fig. 10 Breakdown methodology applied to present-day temperature biases.

a Ensemble means of BC, WCd and WC(phi) contributions to winter biases (HIST-EOBS).

b Relative contributions of BC, WCd and WC(phi) terms to the model dispersion in winter biases. These three maps sum as 100 %.

c–d Same as a–b for summer

Cattiaux et al. (2013)

biases/changes in large-scale dynamics only have a minor contribution to ensemble mean temperature biases/changes

circulation changes are not the main driver of the projected European warming by the end of the twenty first century—, they substantially contribute to the inter-model spread, especially in winter.

model discrepancies in temperature responses are associated with the dispersion in the **North-Atlantic SST** response for both seasons, and with the **snow cover** reduction in winter, and the **cloudiness reduction** in summer.

Cattiaux et al. (2013)

RCMs
and physics

RCMs performance

Resolution dependency

Sensitivity to model physics (parameterizations)
Boundary layer schemes
Deep and Shallow Convection parameterizations
Microphysics schemes
Radiation schemes
Land surface models

Dependency on domain settings and the lateral forcing conditions (nudging)

Long simulations - Flaounas et al. (2011)

6 members
50 km resolution ensemble over west Africa

3 cu schemes
2 PBL schemes.

6 months simulations

Grell ensemble (GR) scheme
Grell 3D ensemble (GR3D) scheme
Kain–Fritsch (KF) scheme

Yosei University scheme (YSU)
Mellor–Yamada–Janjic (MYJ) scheme

Regional climate modelling of the 2006 West African monsoon: sensitivity to convection and planetary boundary layer parameterisation using WRF

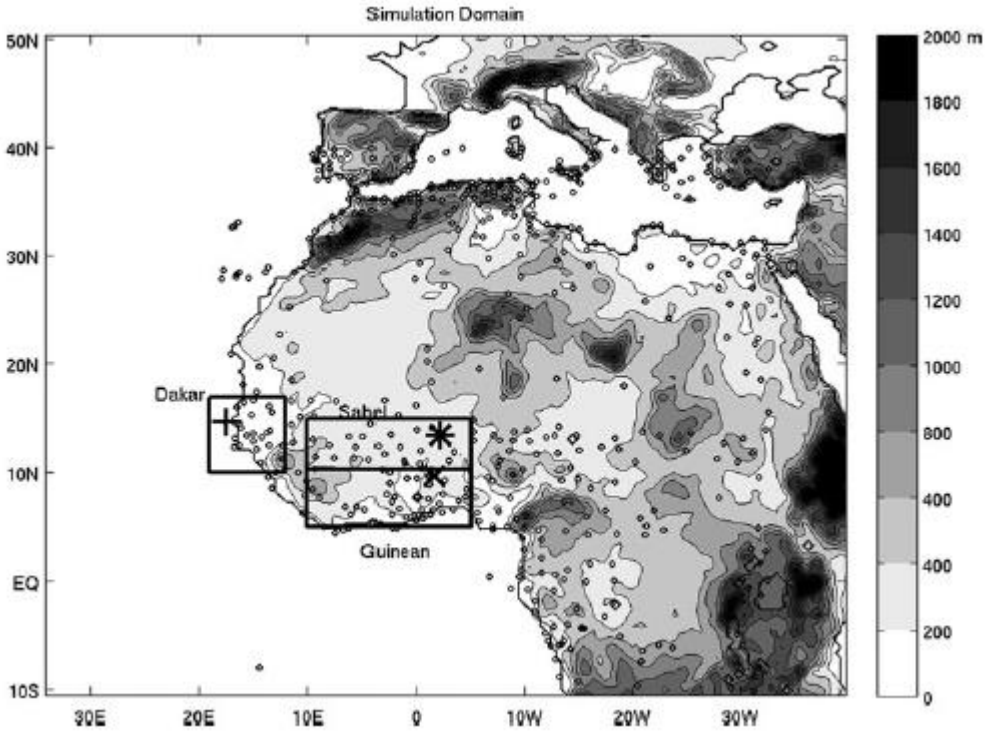

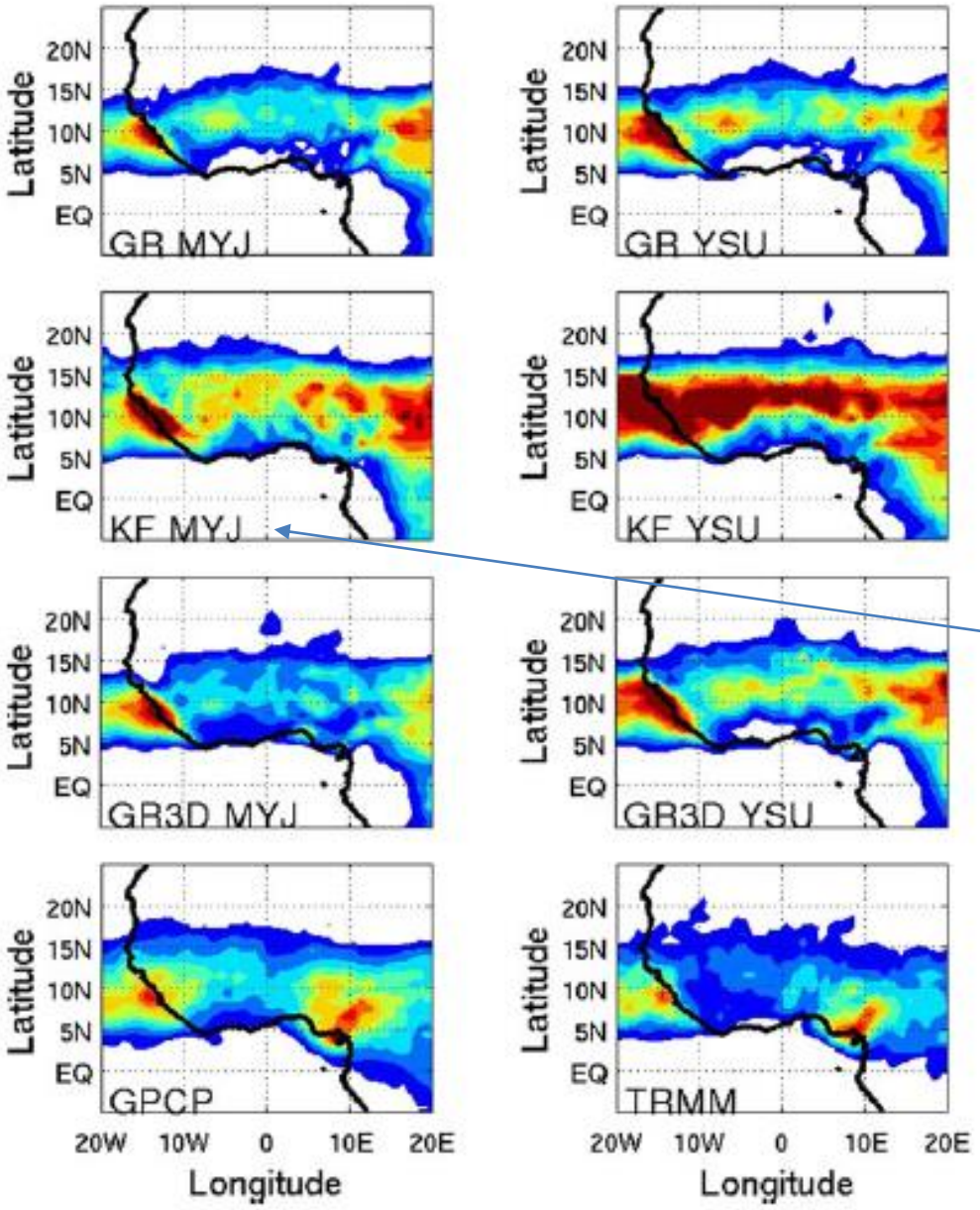

Fig. 2 Mean post-onset rainfall for the six WRF simulations and the GPCP and TRMM products

Sahelian rainy season (July 10th to September 30th)

two main maxima locations: one in the western coast at 5N–10N and over the Fouta Djalon mountains and another one over the Cameroon mountains (10E, 5N–7N)

Flaounas et al. (2011)

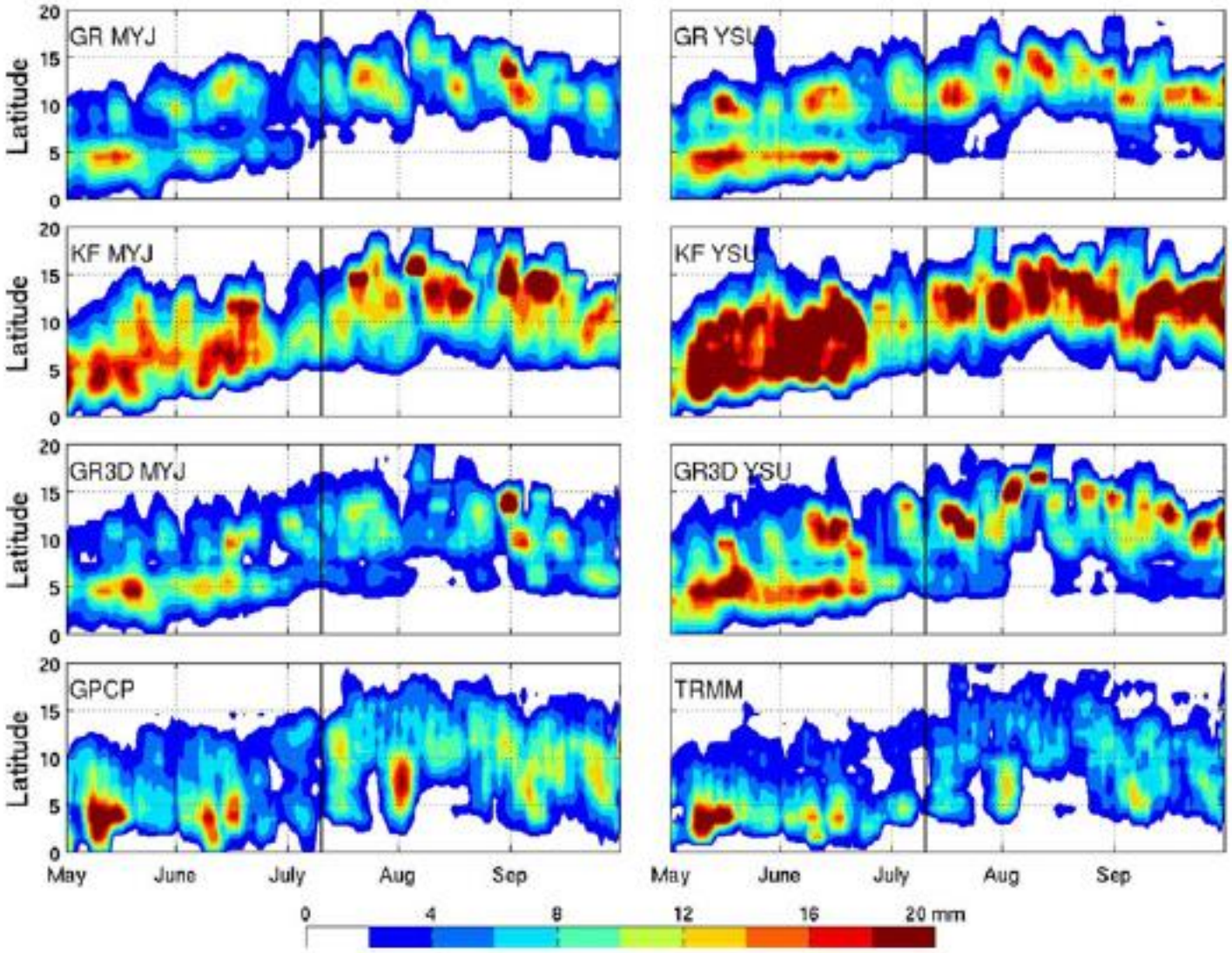

Fig. 3 Hovmoller diagrams of precipitation for the six WRF simulations and the GPCP and TRMM products. Precipitation is averaged between 8.5W and 8.5E. Intense day-to-day variability is eliminated by applying a moving average of ±2 days. Thick black line represents the reference date of the WAM onset (July 10th)

Flaounas et al. (2011)

Over a season the PBL schemes had the strongest effect on temperature, humidity vertical distribution and rainfall amount.

The cu schemes had the largest impact on the dynamics and the rainfall variability.

Overall they found that the combination of the Kain-Fritsch cu scheme and the Mellor-Yamada-Janjic PBL scheme provided the best simulation of the west African monsoon.

The Betts-Miller-Janjic cu scheme was not tested in this study.

Flaounas et al. (2011)

‘‘Super-parameterization’’: A better way to simulate regional extreme precipitation?

One possible approach to improve the interaction of subgrid-scale physical processes and large-scale climate is to replace the conventional convective parameterizations with a high-resolution cloud-system resolving model

‘‘super-parameterized’’ Community Atmosphere Model (SP-CAM) utilizing this approach is used to investigate the distribution of extreme precipitation in the United States

1.875^{o} latitude x 2.5^{o} longitude and 28 vertical levels
2 km horizontal resolution (CRM)

CAM vs SPCAM (reference CPC precipitation observations)

Li et al. 2012

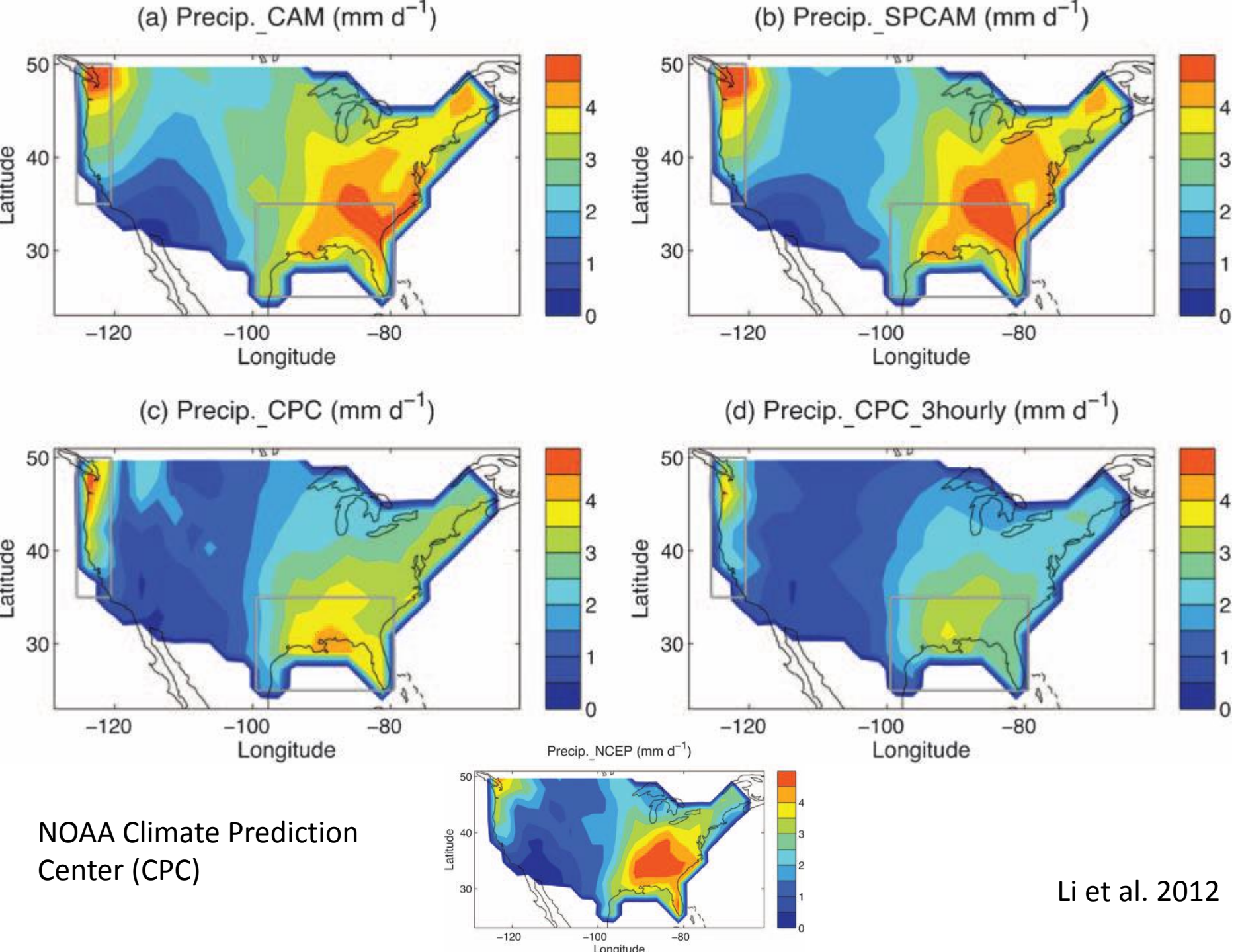

NOAA Climate Prediction Center (CPC)

Li et al. 2012

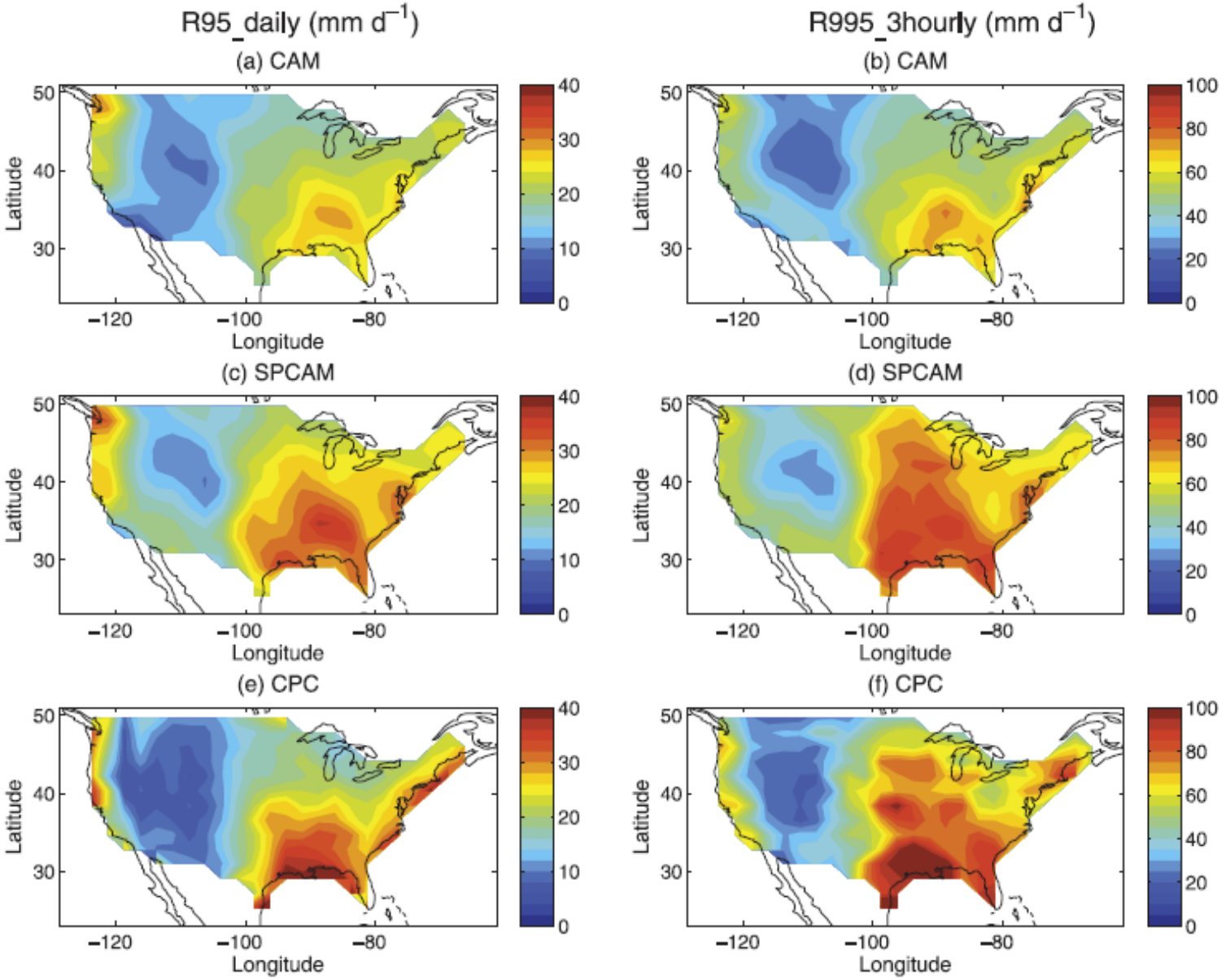

Percentiles
95 daily
99.5 3h

Li et al. 2012

• more extreme precipitation is simulated by SP-CAM than by CAM over almost all the CONUS region despite both models simulate very similar distributions of mean precipitation.

• SP-CAM is much better agreement than CAM in both the spatial distribution and intensity of extreme precip., especially at very high rain rates (99.5% p) and short (3-hourly) time scales.

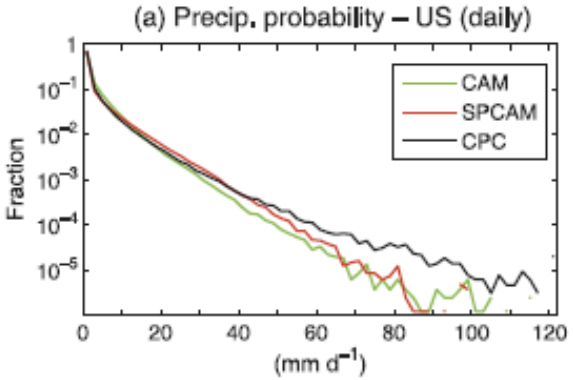

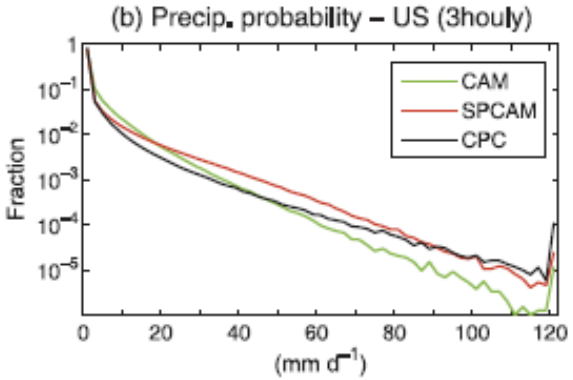

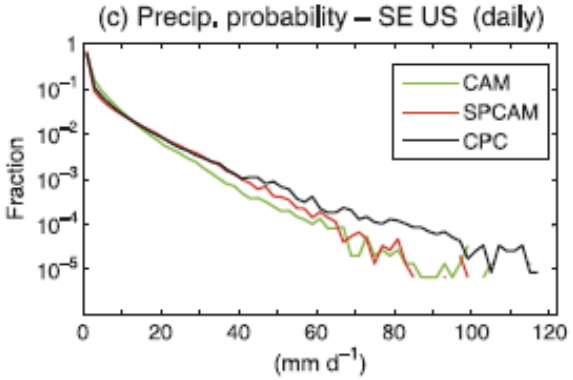

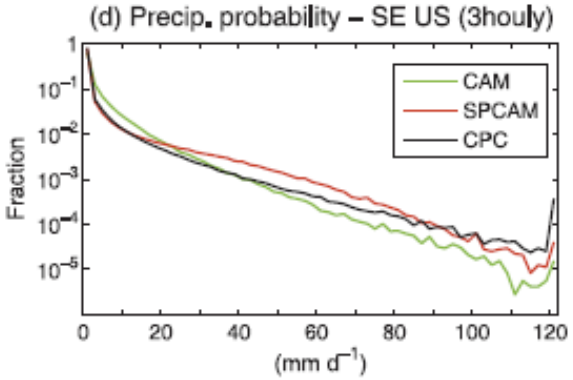

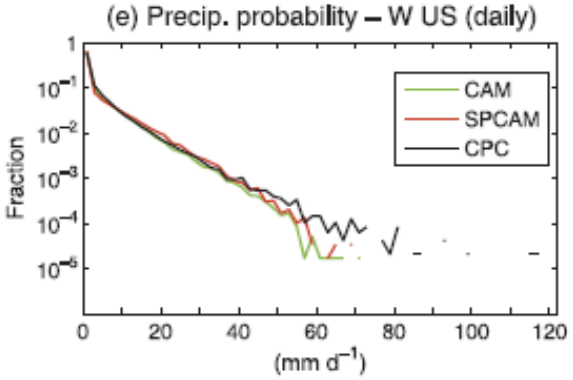

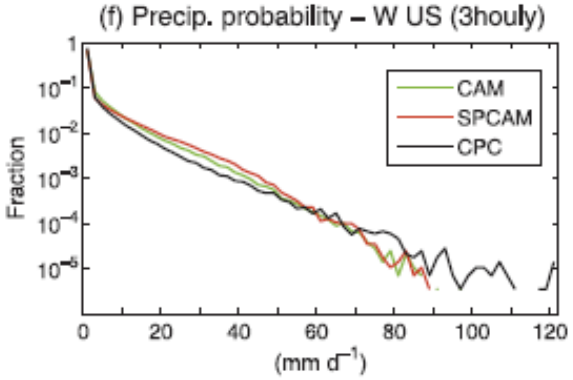

Li et al. 2012

Precipitation pdf shows that the distribution produced by SP-CAM generally agrees with the CPC observations better than that produced by CAM.

SP-CAM simulates more light precipitation and more heavy precipitation at 3-hourly time scales, although the ability of SP-CAM to simulate very extreme precipitation (e.g., daily rates in excess 60 mm) remains limited.

Seasons

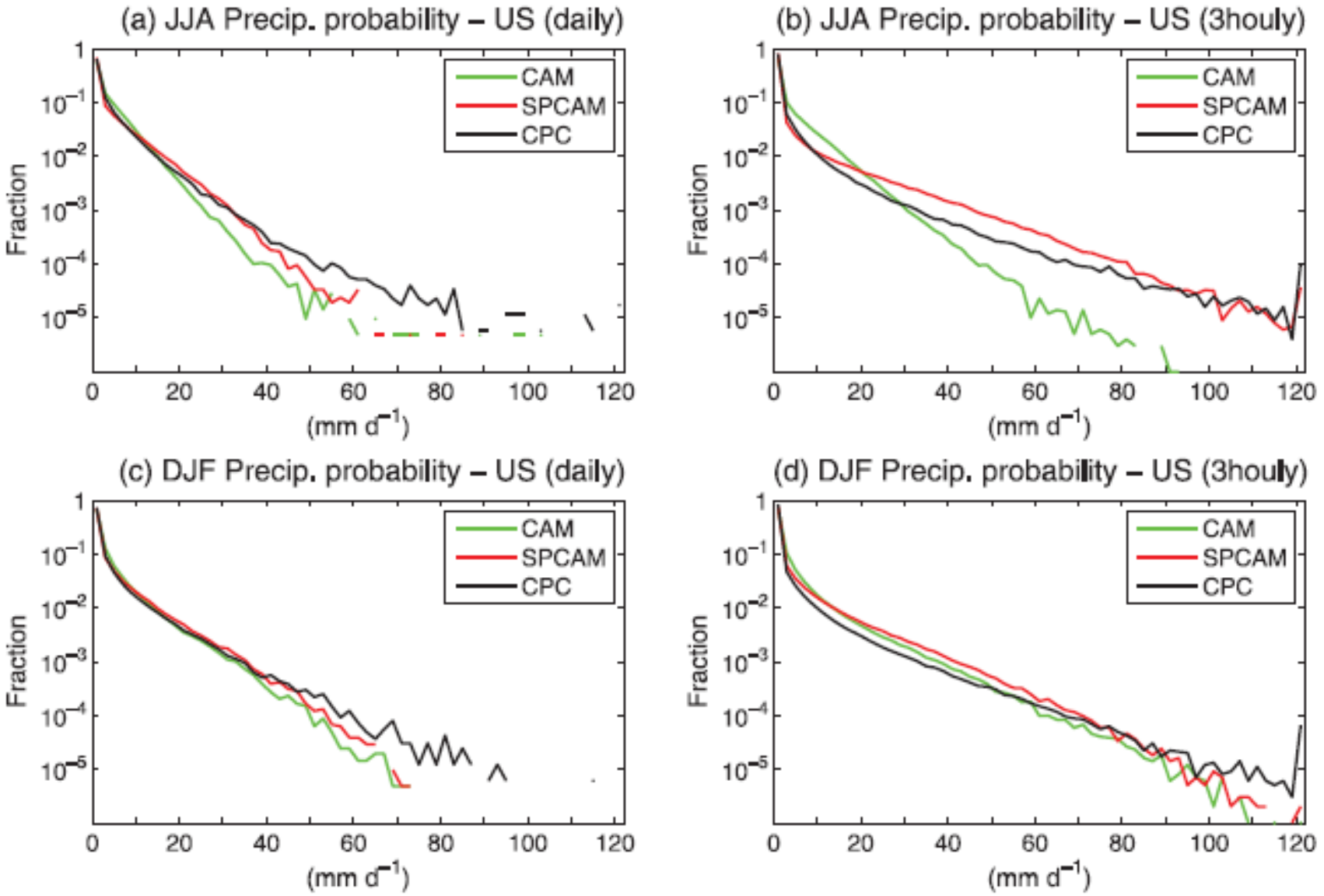

During the convective dominated summer season, SP-CAM clearly outperforms CAM, particularly at 3-hourly time scales

Li et al. 2012

Li et al. 2012

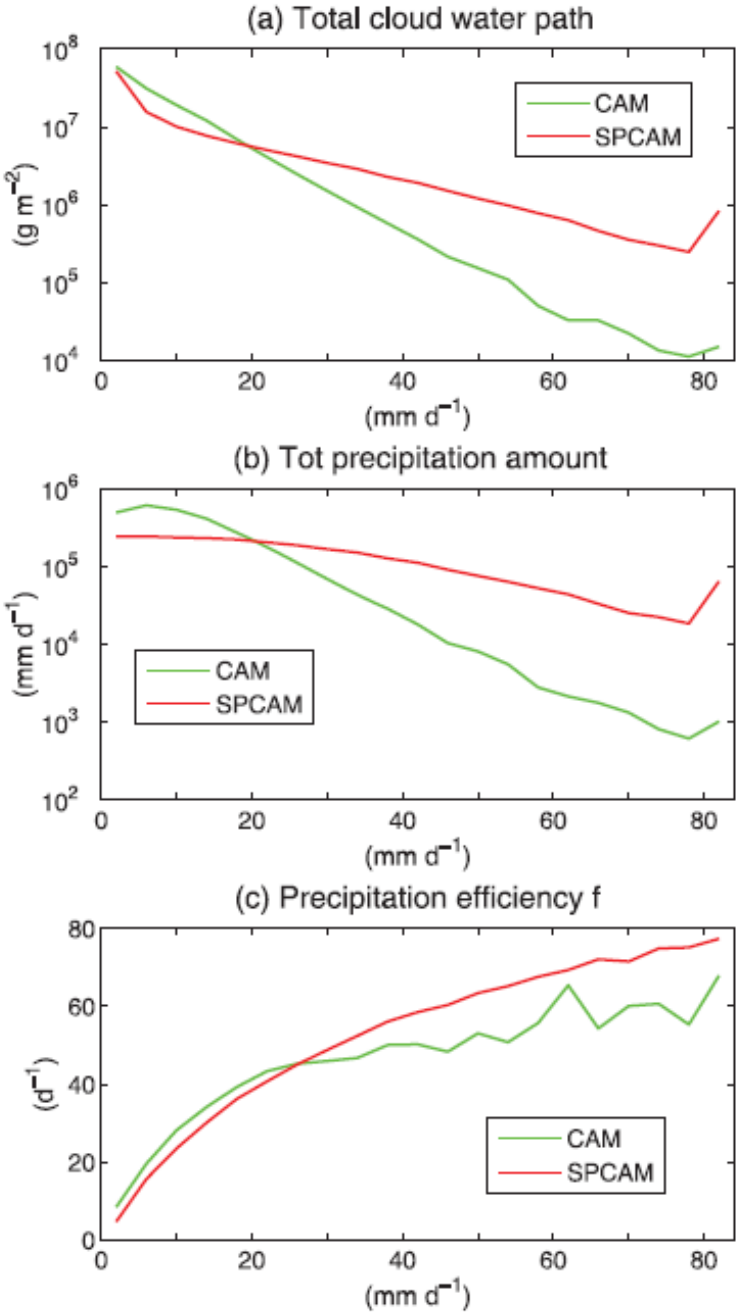

The subgrid dynamics and physics are purported to be better resolved at the cloud scale and hence potentially more realistic in SP-CAM,

Several subgrid processes could potentially result in the more extreme precipitation produced by SP-CAM, including moisture advection, cloud condensation, and the conversion from cloud water to precipitation.

SP-CAM has somewhat higher cloud-water-to-precipitation conversion efficiency than CAM for moderate to high precipitation and that the greater efficiency contributes to some of the improvement of SP-CAM in simulating extreme precipitation.

f defined as the ratio of precipitation rate to the total grid box cloud water path

SP-CAM better simulates the distributions of both light and intense precipitation compared to the standard version of CAM based upon conventional parameterizations.

The improvements are mostly seen in regions dominated by convective precipitation, suggesting that super-parameterization provides a better representation of subgrid convective processes.

Li et al. 2012

Convection => soil-moisture precip feedback

Previous studies suggest EUROPE has positive soil-moisture precipitation feedback.

APPROACH: Test mean diurnal cycle of precipitation in July simulations with perturbed (wet, dry) initial soil moisture.

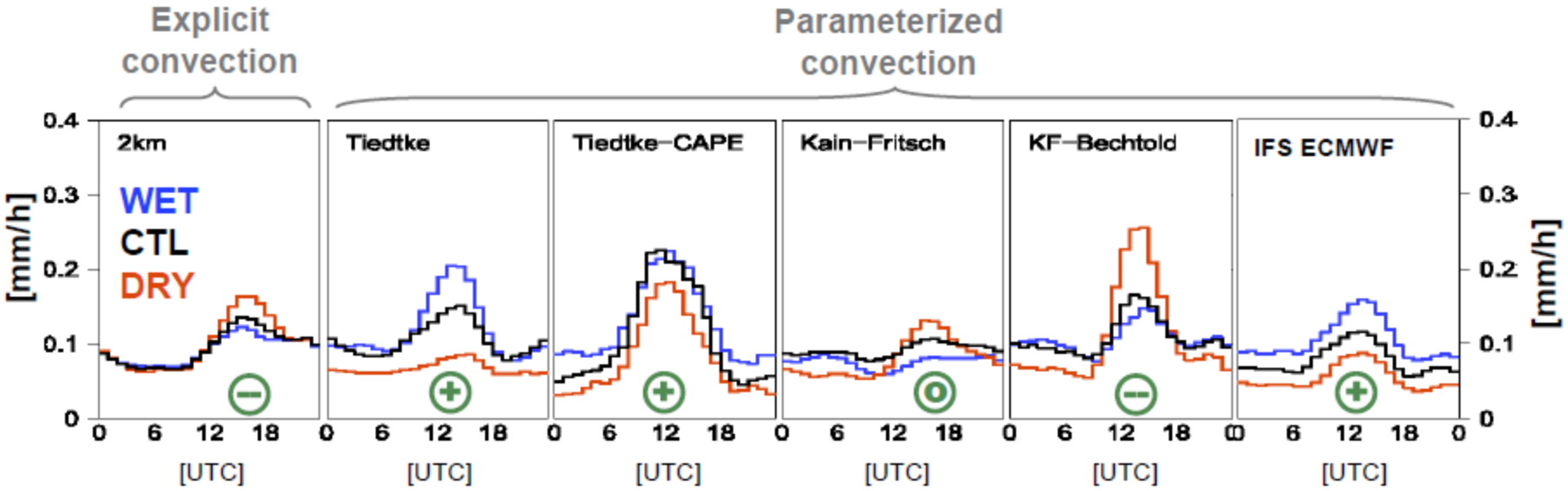

=> Dramatic differences between explicit and parameterized convection, and between different schemes!

=> Convection governs sign of feedback!

(Hohenegger et al, 2009; Brockhaus et al. 2010)

Douglas…